RESEARCH ARTICLE | OCTOBER 16 2024

A spin–flip study of the diradical isomers of pyrrole, furan, and thiophene $\ensuremath{ igoldsymbol{arphi}}$

Zhijian Chen ¹ ; Sebastian Mendoza-Gomez; Jean E. Azar-Tanguay; Christine M. F. Ancajas ¹ ; Dominic A. Sirianni ¹ ¹ ¹ ; Carol A. Parish ¹ ¹ ¹



J. Chem. Phys. 161, 154304 (2024) https://doi.org/10.1063/5.0233736





Articles You May Be Interested In

Low-energy electron collisions with thiophene

J. Chem. Phys. (May 2013)

Low-energy electron scattering from the aza-derivatives of pyrrole, furan, and thiophene

J. Chem. Phys. (June 2013)

Spin-conserving and spin-flipping equation-of-motion coupled-cluster method with triple excitations

J. Chem. Phys. (August 2005)

Challenge us.

What are your needs for periodic signal detection?



Find out more





A spin-flip study of the diradical isomers of pyrrole, furan, and thiophene

Cite as: J. Chem. Phys. 161, 154304 (2024); doi: 10.1063/5.0233736 Submitted: 16 August 2024 • Accepted: 25 September 2024 •







Zhijian Chen,¹ 📵 Sebastian Mendoza-Gomez,¹ Jean E. Azar-Tanguay,¹ Christine M. F. Ancajas,¹ 📵

Dominic A. Sirianni, 2,a) Dand Carol A. Parish 1,a)

Published Online: 16 October 2024

AFFILIATIONS

- Department of Chemistry, Gottwald Center for the Sciences, University of Richmond, Richmond, Virginia 23173, USA
- ²Department of Natural Sciences, Daemen University, Amherst, New York 14226, USA
- ^{a)}Authors to whom correspondence should be addressed: dsiriann@daemen.edu and cparish@richmond.edu

ABSTRACT

Heteroaromatic species are commonly found in complex gaseous mixtures, from tobacco smoke to petroleum and asphaltene combustion products. At high temperatures, C–H bond rupture produces various dehydro radical isomers. We have used the spin-flip formulation of equation-of-motion coupled cluster theory with single and double substitutions (EOM-SF-CCSD) to characterize the energies and wave functions of the lowest lying singlet and triplet states of the diradical (2,3), (2,4), (2,5), and (3,4) di-dehydro isomers of pyrrole, furan, and thiophene. In all cases, these diradicals are minima on the broken-symmetry ω B97X-D/cc-pVDZ potential energy surface. In most cases, the diradical geometries distort to enhance through-space or through-bond coupling in the singlet states and to avoid Coulombic or exchange repulsion in the triplet states. EOM-SF-CCSD results indicate that all diradical isomers are two-configurational, closed shell singlet states. The only exceptions to this are for (2,3) and (2,4) thiophene and (2,3) pyrrole, which each contain more than two configurations. In all cases, the leading term in the multiconfigurational diradical wave function doubly occupies the symmetric radical σ orbital, indicative of either through-space or 1,3 through-bond coupling. We utilized the nucleus-independent chemical shift (NICS) approach to qualitatively assess aromaticity and find that this property varies and may be related to the energetic splittings in these diradical isomers.

Published under an exclusive license by AIP Publishing. https://doi.org/10.1063/5.0233736

I. INTRODUCTION

While tobacco has been widely known to cause cancer for over twenty years, it has only recently been determined that the compound benzo(a) pyrene (BaP) present in cigarette smoke induces DNA damage similar to the genetic mutation patterns found in smoking-related lung cancers.^{1,2} However, the specific molecular mechanism linking aromatic and heteroaromatic compounds present in tobacco smoke to the initiation and progression of a variety of cancers is not well understood. This is partially due to the complexity of tobacco smoke, where each of over 7000 components³ has the potential to interact with the smoker's cells in unexpected, often dangerous ways. This complexity is further heightened by the chemical reactions and decompositions that take place in the components of tobacco at the elevated temperatures associated with smoking. One class of molecules whose chemical and biological activity is relatively well understood is free radicals, which are produced in high concentrations during the combustion of tobacco.4

Spectroscopic identification of the free radicals present in tobacco smoke poses a significant challenge due to the complex nature of the mixture. The most successful approach leverages electron paramagnetic resonance (EPR) spectroscopy, 6 whereby the spin of the unpaired radical electron is used to quantify radical concentration. Due to their short lifetimes and high reactivity, it is necessary to first trap the primary gas-phase radicals to form spin adducts, which are sufficiently long-lived to be analyzed via EPR. Recently, Goel et al. developed the first standardized EPR-based free radical quantification procedure for the analysis of tobacco smoke and identified that the absolute per-cigarette quantities of both gaseous and particulate radicals (6.2 nmol and 65 pmol, respectively) were comparable to the amounts of other carcinogenic gaseous and particulate radicals in tobacco smoke such as nitromethane (9.8 nmol) and benz[a]anthracene (117 pmol), respectively. Despite this, the US Food and Drug Administration (FDA) does not recognize free radicals as hazardous and potentially hazardous chemicals (HPHCs) present in tobacco smoke, which Goel et al. attribute to the analytical challenges associated with their quantification. The development of novel analytical techniques to facilitate the detection of free radicals in tobacco smoke is, therefore, of significant interest in the scientific and human health fields. To promote the direct detection of free radicals in tobacco smoke and subsequent understanding of the carcinogenic and toxicant properties of these species, theoretical approaches are highly complementary to experimental methods. Unlike experimental analysis, computational characterization of these species is not constrained by either their short lifetimes or low concentrations. In particular, quantum chemistry has been used to support the spectroscopic characterization of analytes in a variety of contexts, from helping to develop an approach to detect explosives via halogen bonding to the identification of C₆₀⁺ in the diffuse interstellar medium.8

Though not faced with the same logistical and detection hurdles as experimental characterization, computational ab initio approaches to describe di-, tri-, and polyradicals do experience unique challenges. 11-20 The charge and multiplicity for most organic molecules (typically neutral singlets) are such that the exact electronic wave function may be reasonably represented by a single Slater determinant of occupied molecular orbitals. Such "wellbehaved" molecules are, therefore, amenable to description by theoretically straightforward single-configurational approaches, e.g., Hartree-Fock molecular orbital theory (HF) and post-HF electron correlation methods as well as Kohn-Sham density functional theory (KS-DFT). For open-shell molecules where one or more electron(s) is (are) unpaired, however, a single configurational wave function is reasonable only for high-spin states where all unpaired electrons are of parallel spin (all spin-up or all spin-down, denoted α and β, respectively), e.g., doublets, high-spin triplets, quintets, etc. The simplest conceptual model for the electronic structure of a diradical places two radical electrons in two nearly degenerate "radical" molecular orbitals. Even this (2e, 2o) model still produces six possible configurations that combine to form four electronic states: two closed-shell singlet (CSS) states; an open-shell, two configurational singlet (OSS); and the three components of the open-shell triplet (with $M_s = -1, 0, +1$). For systems where there is only moderate energetic splitting of the radical orbitals, the two closed shell singlets may further mix to produce a pair of two-configurational closed-shell singlet states, TCS(+) and TCS(-). In such "diradicaloid" species (in the vocabulary of two excellent reviews of diradicals, Refs. 21 and 23), the only wave functions that are single configurational are the $M_s = -1$ and $M_s = +1$ components of the triplet, while all the low-spin states [viz., TCS(+) and TCS(-), OSS, and $M_s = 0$ component of the triplet are formally two-configurational. In real molecules with more than two electrons and two orbitals, these low-spin states are likely to be multiconfigurational, i.e., with many configurations contributing nontrivially to the total wave function. To examine these states rigorously necessitates multiconfigurational self-consistent treatment (MCSCF) in combination with a post-MCSCF multireference (MR) treatment of dynamical electron correlation, 24-33 which have been applied successfully to describe the electronic structures of a variety of organic and inorganic di- and polyradicals.1

If, however, a diradicaloid molecule can be reasonably represented within the (2e, 2o) model, a somewhat qualitative alternative to such a multiconfigurational/multireference treatment is the broken-symmetry approach,³⁹ whereby the HOMO and LUMO

of a single-configurational reference are mixed during the selfconsistent field (SCF) procedure. Most commonly combined with DFT (denoted BS-DFT), this approach has become routinely applied to semiquantitatively characterize both the energies and geometries of diradicaloids that, due to either size or complexity, are not amenable to a fully multireference treatment.⁴³ Finally, if a higher level of accuracy than BS-DFT is still needed while maintaining the desired relative simplicity of a single-reference approach, spin-flip formulations of time-dependent density functional theory (SF-TDDFT), 45-49 configuration interaction (SF-CI), 50-52 and equation-of-motion coupled cluster theory (EOM-SF-CC) access formally multiconfigurational low-spin states by performing a spin-flipping excitation on a single-configurational (typically high-spin triplet) reference. Among these methods' original use cases, a variety of organic and inorganic diradical systems have been explored with spin-flip approaches, 22,4 ² including recent efforts by some of us.

In this study, we investigate the molecular geometries and electronic structures of the twice dehydrogenated diradical isomers of furan, pyrrole, and thiophene (Fig. 1), which are representative model systems for the wide variety of polycyclic aromatic hydrocarbons (PAHs) present in tobacco smoke. We have employed BS-UDFT to obtain optimized structures and vibrational frequencies for the lowest singlet (S1) and lowest triplet (T1) states of these species. Furthermore, we have characterized the energies and wave functions of these states and singlet/triplet splittings via EOM-SF-CCSD. Analysis of the natural orbitals (NOs) of spin-flipped singlet states reveals the classic through-bond coupling of radical lobes originally described by Hoffmann,⁶⁵ showcasing both these species' diradical nature and the source of their electronic stabilization. Finally, we have characterized the aromaticity for these diradicals using the nucleus-independent chemical shift (NICS) approach, 66-69 whereby we find that aromaticity plays a supporting role in these molecules' notable stability and explains the planar structures observed in all optimizations. It is our hope that our

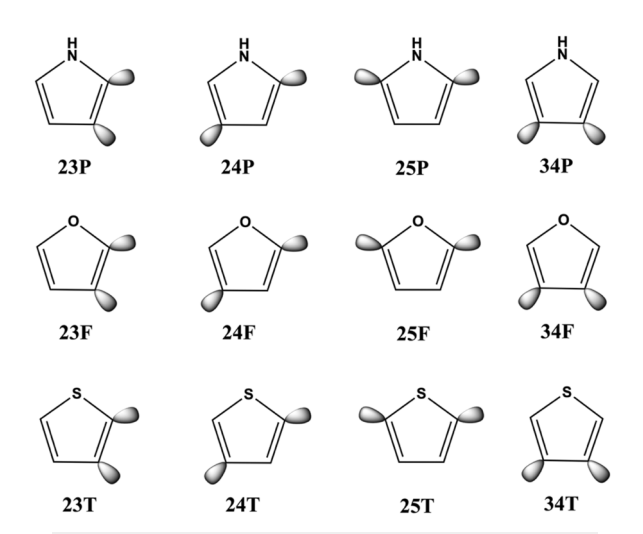


FIG. 1. Heteroaromatic diradical isomers characterized in this study.

characterization of the lowest energy ground states and geometries, along with electronically excited triplet states, will support future spectroscopic identification of aromatic diradicals in tobacco smoke.

II. METHODS

For all diradical isomers of the heteroaromatic molecules furan, thiophene, and pyrrole, the molecular geometries of the lowestenergy triplet and singlet states were optimized using the ωB97X-D functional 70,71 and the cc-pVDZ basis set 72 with an unrestricted Kohn-Sham (UKS) reference determinant. To approximately target the structure of the unpaired diradical singlet state for each isomer, the broken symmetry approach was utilized (BS-UKS) by equally mixing the HOMO and LUMO Kohn-Sham orbitals in the reference. The only exceptions are for the lowest diradical singlet (S₁) states of 23P, 25P, and 25F, which were optimized using unrestricted coupled cluster theory with single and double substitutions (UCCSD) and a broken-symmetry unrestricted Hartree-Fock (BS-UHF) reference determinant in the same ccpVDZ basis set. All optimized geometries were confirmed as true minima on their respective potential energy surfaces via frequency analysis, performed at the same level of theory as the geometry optimizations.

The wave functions for the lowest energy singlet states of each diradical isomer were constructed using the spin-flip formulation of equation-of-motion coupled cluster theory with single and double substitutions (EOM-SF-CCSD) in the cc-pVDZ basis set. This approach accesses these formally multiconfigurational electronic states within the context of a single configurational theory by applying a spin-flipping excitation operator to the high-spin $(M_s = +1)$ component of the open-shell triplet reference, which we prepared for each isomer at the UHF/cc-pVDZ level of theory by ensuring that the radical orbitals σ and σ^* (or S and A in Hoffmann notation,⁷³ respectively) were singly occupied by α electrons. Once the appropriate UHF reference was prepared, EOM-SF-CCSD was applied to generate a range of excited states, the lowest energy of which were fully characterized by (i) their singlet-triplet splittings, i.e., the energy difference between the spin-flipped low-spin state and the high-spin reference configuration at the CCSD/cc-pVDZ level of theory; (ii) examining their orbital transitions and amplitudes to determine the identity of the state; (iii) computing their spin-squared expectation values, $\langle S^2 \rangle$, to identify the presence of any spin-contamination; and (iv) constructing their natural orbitals to facilitate their chemical interpretation (further details on reference state preparation and analysis of the spin-flipped excited states is presented in Sec. S-II of the supplementary material). Despite the possibility that these unrestricted computations may suffer from spin contamination, we have utilized unrestricted references in all spin-flip computations (i.e., at the EOM-SF-UCCSD level of theory) to allow for direct comparison of our results with cyclopenta-2,4-dien-1-id-2,5-ylene, the all-carbon anionic analog of these heteroaromatic 2,5-diradical isomers, which has been previously examined by some of us as a product of the Bergman-type cyclization of penta-1,4-diyn-3-ide.⁶⁴ All geometry optimizations, frequency analyses, and spin-flip computations were performed using Q-Chem version 5.4,74 whose default molecular orientation results in symmetry labels, which do not conform to the Mulliken

convention; we have converted all symmetry labels in this work to conform to Mulliken conventions to facilitate consistency with the literature. Finally, the presence of aromaticity in the S_1 geometries for all isomers was assessed with isotropic nucleus-independent chemical shift (NICS) computations within the gauge-invariant atomic orbital (GIAO) formalism 75,76 at the B3LYP/6-311++ G^{**} level of theory with a BS-UKS reference using Gaussian 16.

III. RESULTS AND DISCUSSION

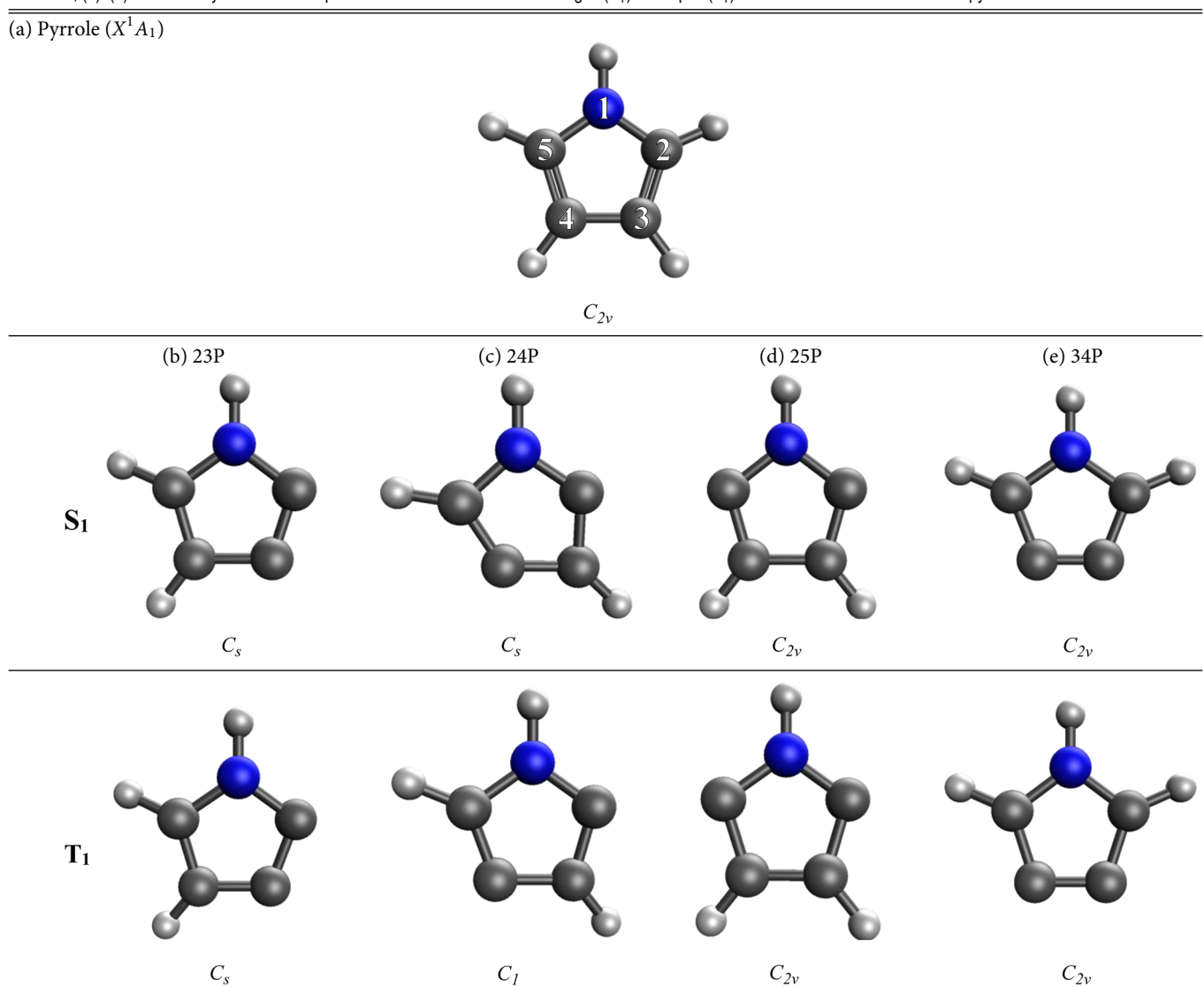
A. Optimized molecular structures of diradical isomers

Presented in Tables I and II are the optimized molecular geometries and geometric parameters of the ground singlet (X^1A_1) state of pyrrole, optimized at the ωB97X-D/cc-pVDZ level of theory with a closed-shell restricted Kohn-Sham (RKS) reference, and the lowest open-shell singlet (S_1) and high-spin triplet (T_1) states for all diradical isomers of pyrrole optimized at this same level of theory (with BS-UKS and UKS references, respectively), except for the S₁ structures of 23P, 25P, and 25F, which were optimized at the BS-UCCSD/cc-pVDZ level. We have limited our geometric discussion in the main text to the diradical isomers of pyrrole because the salient features of these structures, as well as their implications for the electronic states of isomers analyzed in Sec. III B below, are also shared with the diradical isomers of thiophene and furan. A complete set of figures visualizing the S₁ and T₁ geometries of all diradical isomers and their geometric parameters (both raw and deviations with respect to parent molecules) are presented in Tables S-I.1-S-I.9 of the supplementary material; finally, the lowest vibrational frequencies for S1 and T1 structures of all isomers are provided in Table S-I.10 in the supplementary material.

1. Adjacent radical centers: Geometries of 2.3- and 3.4-diradical isomers

For diradical isomers with adjacent radical centers [i.e., the 2,3diradical and 3,4-diradical isomers; Tables I(b), I(e), II(b), and II(e)], the most striking geometric feature is the notable shortening of the C–C bond length between the radical centers in the structures of the S_1 state. For example, R_{23} contracts by between -0.05 and -0.10 Å for the S₁ state of all 2,3-diradicals, while the corresponding bond length R_{34} shortens by between -0.15 and -0.16 Å for the S_1 state of 3,4-diradicals. These geometric differences are most likely due to the coupling of radical electrons within the ring plane via spatial overlap of their molecular orbitals (a "through-space" coupling), thereby increasing the effective bond order between radical centers beyond what would normally be expected due to aromatic delocalization. On the other hand, triplet geometries for 3,4-diradical isomers either do not display as significant a bond-length shortening as their singlet counterparts (e.g., -0.09 vs -0.16 Å for T_1 and S_1 states of 34F, respectively) or exhibit a nonsignificant lengthening (+0.001 Å for the T_1 state of 34T). For 2,3-diradical triplet isomers, all exhibit an increase in the distance between adjacent radical centers vs the parent structure of up to +0.09 Å for the T_1 state of 24F. This behavior likely results from both the Coulombic and exchange repulsion felt between these parallel-spin radical electrons, where the favorable through-space coupling and subsequent "bond" formation present in S₁ states is spin-forbidden.

TABLE I. (a) Molecular symmetry and optimized structure for the X^1A_1 state of the pyrrole parent molecule, optimized at the ω B97X-D/cc-pVDZ level of theory with a RKS reference; (b)–(e) molecular symmetries and optimized structures for the lowest singlet (S₁) and triplet (T₁) states of each diradical isomer of pyrrole.



2. Non-adjacent radical centers: Geometries of 2,4- and 2,5-diradical isomers

Despite being separated by two intervening σ bonds, the S_1 structures for all 2,4-diradical isomers also exhibit a shortening of the intraradical $C_2 \cdots C_4$ distance (R_{24}) of -0.30, -0.16, and -0.32 Å for **24F**, **24T**, and **24P** (differences relative to the parent molecule; data shown in Tables S-I.3 and S-I.6 of the supplementary material and Table II of the main text, respectively). Just like for the 2,3-diradical isomers, this is an indication of the importance of through-space coupling for these molecules, supported by the fact that the T_1 structures for these isomers display markedly different geometries, with R_{24} decreasing by only -0.05 Å in **24P** and actually *increasing* by +0.04 and 0.03 Å in **24F** and **24T**, respectively.

Coupling of the radical centers in 2,4-diradical isomers is not only possible through spatial overlap but also via interactions with the intervening σ bonding network in the ring, which defines the classic "through-bond" coupling originally described by Hoffmann. ^{65,73} The radical electrons in 2,4 isomers can couple with one another through either a "1,3" or "1,4" interaction (using Hoffmann's notation). These coupling pathways pass through either the two intervening σ bonds (between $C_2-C_3-C_4$) or through the three intervening σ bonds (between $C_2-X-C_5-C_4$; X=N, O, S), respectively. It has been hypothesized that the through-bond coupling strength in a 1,3-coupling motif increases as the intervening bond angle (here, \angle 234) becomes more acute; ⁷⁸ however, we will forego such finegrained interpretation of our geometric deviations in favor of the wave function and orbital analyses in Sec. III B below.

TABLE II. (a) Bond lengths (Å) and angles (°) for optimized structure of the X^1A_1 state of the pyrrole parent molecule, optimized at the ω B97X-D/cc-pVDZ level of theory with a UKS reference; and (b)–(e) differences in bond lengths (Å) and angles (°) for the lowest singlet (S₁) and triplet (T₁) states of each diradical isomer of pyrrole, computed as diradical minus parent value.

	(a) Pyrrole	(b)	23P	(c)	24P	(d)	25P	(e)	34P
Parameter	X^1A_1	$\overline{S_1}$	T ₁	S_1	T ₁	$\overline{S_1}$	T ₁	$\overline{S_1}$	T ₁
R ₁₂ (Å)	1.37	+0.01	-0.00	+0.00	-0.01	+0.00	-0.00	+0.02	+0.01
R_{23} (Å)	1.38	-0.05	+0.02	-0.01	+0.01	+0.01	+0.04	+0.00	+0.05
R_{34} (Å)	1.42	+0.02	-0.02	-0.05	-0.01	+0.02	-0.03	-0.15	-0.09
R_{45} (Å)	1.38	+0.02	+0.01	-0.00	-0.01	+0.01	+0.04	+0.00	+0.05
R_{51} (Å)	1.37	+0.02	+0.01	-0.01	+0.02	+0.00	-0.00	+0.02	+0.01
R_{24} (Å)	2.26	-0.00	+0.04	-0.32	-0.05	-0.01	-0.00	-0.07	-0.03
R_{25} (Å)	2.24	-0.01	+0.00	-0.09	-0.01	-0.06	-0.02	0.03	-0.04
∠123 (°)	107.7	-1.9	-2.0	+14.1	+2.6	+4.4	+0.5	-4.1	+1.7
∠234 (°)	107.3	+4.9	+2.9	-17.6	-3.5	-1.9	-0.6	+4.0	+0.4
∠345 (°)	107.3	-6.6	-2.5	+16.8	+3.4	-1.9	-0.6	+4.0	+0.4
∠451 (°)	107.7	+1.5	+1.4	-7.9	-1.7	+4.4	+0.6	-4.1	+1.7
∠512 (°)	109.9	-3.7	-0.5	-5.5	-1.6	-5.1	-1.1	+0.1	-4.2

Unlike the 2,3- and 2,4-diradical isomer geometries, which vary from their fully saturated parent molecule in a uniform fashion regardless of the heteroatom, the geometric features of 2,5-diradical isomers are unique to each heteroaromatic molecule. For 25T, R_{25} shortens greatly by -0.32 Å and lengthens insignificantly by +0.002 Å for the S₁ and T₁ states, respectively. This geometric deviation is most likely the result of a through-space coupling of the radical electrons, as the narrowing of $\angle 512$ by -11.7° in the S_1 structure should maximize their spatial overlap. For 25F and 25P, however, the intraradical $C_2 \cdot \cdot \cdot C_5$ distance decreases by no more than -0.06 Å in either the S_1 or T_1 structures; these changes are predominantly mediated by a narrowing of $\angle 512$ and $\angle 234 = \angle 345$. While the narrowing of $\angle 512$ is of similar magnitude in the S₁ and T_1 structures of these two isomers, the deviation in $\angle 234$ of more than -11° for both S_1 and T_1 structures of 25F is significantly larger than the same deviations of -1.8° and -0.6° for S_1 and T_1 structures of 25P, which is mirrored by a slight lengthening of the C₃-C₄ bond in both structures of 25F vs a slight shortening of the same bond in 25P. The very small decrease of R_{25} in 25F indicates minimal through-space coupling, while the flattening of ∠512 may suggest the importance of 1,4 through-bond coupling in this isomer. These geometric distortions are too subtle to reliably interpret on their own but will play a supporting role in the analyses of Sec. III B below to help identify the specific coupling motifs present between the radical electrons in these isomers.

Finally, the markedly greater shortening of R_{25} and narrowing of \angle 512 exhibited by the S_1 structure of **25T** vs the S_1 structures **25P** and **25F** are due most likely to the different properties of the heteroatoms themselves. Specifically, the sulfur 3s- and 3p-like valence atomic orbitals are more diffuse than the 2s- and 2p-like valence atomic orbitals occupied by O and N. This allows \angle 512 in **25T** to enjoy more angular flexibility vs **25P** and **25F**, which is, therefore, able to better accommodate the geometric distortions necessary to maximize both through-space and 1,3 through-bond radical coupling. This is supported by the structure of the ground-state singlet

 (X^1A_1) , hereafter S_0) of cyclopenta-2,4-dien-1-id-2,5-ylene (cf. Fig. S-3 in the supplementary material of Ref. 64), where the corresponding bond angle of 97° compares much more closely with the values of 102.4° and 112.5° for \angle 521 of **25F** and **25P**, respectively, whereas the \angle 521 is significantly more acute in the S_1 structure of **25T** at 80.0° .

B. Electronic structures of diradical isomers

We have characterized the wave function of the lowest energy singlet state at the S₁ structure of each isomer with the spin-flip formulation of equation-of-motion coupled cluster theory (EOM-SF-UCCSD) with the cc-pVDZ basis set. This approach requires the initial preparation of a high-spin triplet reference determinant such that the singly occupied molecular orbitals (SOMOs) correspond to the symmetric (σ) and antisymmetric (σ^*) combinations of nonbonding radical orbitals within the ring plane (see Tables S-II.A.1-S-II.C.4 in the supplementary material for frontier molecular orbital visualizations, symmetry labels, and chemical designations for all diradical isomers). For all EOM-SF-CCSD computations, this triplet reference was constructed with unrestricted Hartree-Fock (UHF) and the cc-pVDZ basis set at the S1 structures described in Sec. III A. Schönflies symbols, total electronic energies (Etot; a.u.), expectation values of the spin-squared operator, (\hat{S}^2) , and leading determinants contributing to the total wave function for both the lowest energy spin-flipped excited singlet and high-spin triplet reference states are shown in Table III. In addition, included in Table III are the vertical spin-flip excitation energies (ΔE_{ST} ; eV), equivalent to the energy difference of singlet minus triplet total energies.

For all isomers, the singlet state lies lower in energy than the triplet state, and all ground state singlet wave functions are multiconfigurational. The leading determinant for the ground state wave function for all isomers is $|(\sigma)^2\rangle$ (i.e., the closed-shell determinant which doubly occupies the symmetric radical σ MO), and with the

TABLE III. Schönflies symbols, total electronic energies, (\$^2\$), and wave functions for high-spin triplet unrestricted Hartree—Fook reference and lowest-energy spin-flipped excited states prepared at the UHF/co-pVDZ and EOM-SF-UCCSD/co-pVDZ levels of theory, respectively, using S₁ structures optimized at the wB97X-D/co-pVDZ level of theory with BS-UKS reference. In addition, provided are vertical spin-flip excitation energies (\(\triangle z_{ex1}\). taken as singlet minus triplet total energies.

meory w	III DO-UNO IE	elerence. In addition, prove	ided are vertical spi	n-IIIp excitation en	theory with b≾-ong leterance. In addition, provided are vertical spiri-hip excitation energies (△EST), taken as singlet minus triplet total energies.
	State ^a	E _{tot} (a.u.)	ΔE_{ST} (eV)	$\langle \hat{S}^2 \rangle$ (a.u.)	Wave function ^{b-d}
23F	$1^3A'$ X^1A'	-227.989 089 42 -227.998 143 82		2.1092 0.0999	$100\% \times (\text{core})^{32} (\sigma)^{\alpha} (\sigma^{*})^{\alpha} \rangle$ $65\% \times (\text{core})^{32} (\sigma)^{\alpha\beta} \rangle + 17\% \times (\text{core})^{32} (\sigma^{*})^{\alpha\beta} \rangle + \dots$
24F	$\frac{1^3A'}{X^1A'}$	-227.959 549 46 -227.991 486 36		2.4922 0.0833	$100\% \times (\text{core})^{32} (\sigma)^{a} (\sigma^{*})^{a} \rangle$ $77\% \times (\text{core})^{32} (\sigma)^{a\beta} \rangle + 9\% \times (\text{core})^{32} (\sigma^{*})^{a\beta} \rangle + \dots$
25F	$\frac{1^3B_2}{X^1A_1}$	-227.992 110 23 -227.999 792 08		2.1384 0.0170	$100\% \times (\text{core})^{32} (\sigma)^{\alpha} (\sigma^{*})^{\alpha} \rangle$ $65\% \times (\text{core})^{32} (\sigma)^{\alpha\beta} \rangle + 17\% \times (\text{core})^{32} (\sigma^{*})^{\alpha\beta} \rangle + \dots$
34F	$\frac{1^3B_2}{X^1A_1}$	-227.96432079 -228.00351334	-1.0665	2.0444 0.0086	$100\% \times (\text{core})^{32} (\sigma)^a (\sigma^*)^a \rangle$ $79\% \times (\text{core})^{32} (\sigma)^{a\beta} \rangle + 8\% \times (\text{core})^{32} (\sigma^*)^{a\beta} \rangle + \dots$
	$1^3A'$ X^1A'	-550.57447618 -550.65661998	-2.2352	2.1496 0.0219	$100\% \times (\text{core})^{40} (\sigma)^{a} (\sigma^{*})^{a} \rangle$ $78\% \times (\text{core})^{40} (\sigma)^{a\beta} \rangle + 3\% \times (\text{core})^{40} (\sigma)^{\beta} (\sigma^{*})^{a} \rangle + 2\% \times (\text{core})^{38} (15a')^{\beta} (\sigma)^{a\beta} (\sigma^{*})^{a} \rangle + 2\% \times (\text{core})^{40} (\sigma)^{a} (\sigma^{*})^{\beta} \rangle + \dots$
24T	$\frac{1^3A'}{X^1A'}$	-550.635 023 95 -550.649 915 95	-0.4052	2.5405	$100\% \times (\text{core})^{40} (\sigma)^{a} (\sigma^{*})^{a} \rangle$ $63\% \times (\text{core})^{40} (\sigma)^{a\beta} \rangle + 8\% \times (\text{core})^{40} (\sigma^{*})^{a} \rangle + 6\% \times (\text{core})^{40} (\sigma^{*})^{a\beta} \rangle + 3\% \times (\text{core})^{40} (\sigma^{*})^{\beta} \rangle + \dots$
25T	$\frac{1^3B_2}{X^1A_1}$	-550.61240528 -550.65025813	-1.0300	2.1032 0.0146	$100\% \times (\text{core})^{40} (\sigma)^a (\sigma^*)^a \rangle$ 77% × $ (\text{core})^{40} (\sigma)^{a\beta} \rangle + 8\% \times (\text{core})^{40} (\sigma^*)^{a\beta} \rangle + \dots$
34T	$\frac{1^3B_2}{X^1A_1}$	-550.613 561 25 -550.655 346 07	-1.1370	2.0451 0.0086	$100\% \times (\text{core})^{40} (\sigma)^{a} (\sigma^{*})^{a} \rangle$ $77\% \times (\text{core})^{40} (\sigma)^{a\beta} \rangle + 3\% \times (\text{core})^{40} (\sigma^{*})^{a\beta} \rangle + \dots$
23P	$1^3A'$ X^1A'	-208.165 455 06 -208.184 213 64	-0.5104	2.0325	$100\% \times (\text{core})^{32} (\sigma)^{\alpha} (\sigma^{*})^{\alpha} \rangle$ $67\% \times (\text{core})^{32} (\sigma)^{\alpha\beta} \rangle + 12\% \times (\text{core})^{32} (\sigma^{*})^{\alpha\beta} \rangle + 2\% \times (\text{core})^{32} (\sigma)^{\alpha} (\sigma^{*})^{\beta} \rangle + 1\% \times (\text{core})^{32} (\sigma)^{\beta} (\sigma^{*})^{\alpha} \rangle + \dots$
24P	$\frac{1^3A'}{X^1A'}$	-208.131 978 48 -208.176 969 61	-1.2243	2.3738	$100\% \times (\text{core})^{32} (\sigma)^{a} (\sigma^{*})^{a} \rangle$ $79\% \times (\text{core})^{32} (\sigma)^{a\beta} \rangle + 3\% \times (\text{core})^{32} (\sigma^{*})^{a\beta} \rangle + \dots$
25P	$\frac{1^3B_2}{X^1A_1}$	-208.168 237 33 -208.181 505 98	-0.3611	2.0824 0.0118	$100\% \times (\text{core})^{32} (\sigma)^a (\sigma^*)^a \rangle$ $68\% \times (\text{core})^{32} (\sigma)^{a\beta} \rangle + 14\% \times (\text{core})^{32} (\sigma^*)^{a\beta} \rangle + \dots$
34P	$\frac{1^3B_2}{X^1A_1}$	-208.142 265 08 -208.187 077 94	-1.2194	2.0266 0.0062	$100\% \times (\text{core})^{32} (\sigma)^{\alpha} (\sigma^*)^{\alpha} \rangle$ $77\% \times (\text{core})^{32} (\sigma)^{\alpha\beta} \rangle + 8\% \times (\text{core})^{32} (\sigma^*)^{\alpha\beta} \rangle + \dots$

Schönflies symbols for electronic states utilize Mulliken conventions for orienting symmetry axes in the $C_{2\nu}$ point group.

^bRelative weights for each Slater determinant are computed as the square of the spin-flip excitation amplitude; determinants with a relative weight smaller than 5% are included only when necessary to demonstrate fidelity to the overall spin state.
^c(core)²ⁿ denotes the first n doubly occupied, lower energy molecular orbitals. When an excitation out of these orbitals occurs, the newly singly occupied orbitals are explicitly shown; see Tables S-II.A.1–S-II.C.4 in

the supplementary material for a complete set of relevant frontier molecular orbitals for all diradical isomers.

^dUnrestricted molecular orbitals are listed from left to right in order of increasing energy; when represented as being "doubly occupied," the energy of the MO in the α manifold is given precedence.

exception of 23T, the corresponding closed-shell $|(\sigma^*)^2\rangle$ determinant (doubly occupying the antisymmetric radical σ^* MO) is the second most significant contributor. Furthermore, for all isomers except 23T, 24T, and 23P, $|(\sigma)^2\rangle$ and $|(\sigma^*)^2\rangle$ are the *only* significant contributors to the ground state wave function, interpretable within the classic (2e, 2o) model (cf. Fig. S-1 in the supplementary material of Ref. 64) as being two-configurational, closed shell singlet (TCS) states,

$$|TCS\rangle = w_1|(\sigma)^{\alpha\beta}\rangle + w_2|(\sigma^*)^{\alpha\beta}\rangle,$$
 (1)

where w_i is the weight of determinant i for the ground state wave functions given in Table III, and where without loss of generality we have ignored the contribution of the doubly occupied core orbitals to each determinant. For 24T and 23P, however, four determinants are significant contributors to the ground state wave function,

$$|X^{1}A'\rangle = w_{1}|(\sigma)^{\alpha\beta}\rangle + w_{2}|(\sigma)^{\beta}(\sigma^{*})^{\alpha}\rangle + w_{3}|(\sigma^{*})^{\alpha\beta}\rangle + w_{4}|(\sigma)^{\alpha}(\sigma^{*})^{\beta}\rangle + \dots$$
 (2)

Two of these leading determinants resemble the TCS of Eq. (1), while the others correspond to the combination of open-shell low-spin (i.e., $M_s = 0$) determinants in a manner akin to an open-shell singlet (OSS) state within the (2e, 2o) picture, namely

$$| \text{ OSS} \rangle = w_1 |(\sigma)^{\beta} (\sigma^*)^{\alpha} \rangle + w_2 |(\sigma)^{\alpha} (\sigma^*)^{\beta} \rangle + \dots$$
 (3)

We can, therefore, think of the ground state $|X^1A'\rangle$ wave function for 24T and 23P as being predominantly a TCS with contributions from an OSS, i.e.,

$$|X^1A'\rangle = c_1|TCS\rangle + c_2|OSS\rangle + \dots,$$
 (4)

where c_1 and c_2 are generic expansion coefficients not connected to the determinant weights w_i provided in Table III. The contribution of this OSS state is symmetry-allowed within the C_s point group (both TCS and OSS states belong to the A' irreducible representation in the C_s point group, the symmetries to which 24T and 23P both optimize), whereas the same phenomenon is symmetry forbidden for all $C_{2\nu}$ -symmetric isomers because the TCS belongs to A_1 but the OSS belongs to B_2 (see, e.g., Table S-II.C.3 in the supplementary material for visualizations of the MOs of 25P, a $C_{2\nu}$ symmetric isomer). The prevalence of TCS states as the ground state for all species (or, at least, where $|(\sigma)^2|$ is the dominant contributor to the total wave function) is not surprising, as the ground state for both p-benzyne and cyclopenta-2,4-dien-1-id-2,5-ylene are known to be TCS. 63,64 Taken together with their geometries discussed earlier, the dominance of the $|(\sigma)^2\rangle$ determinant in the wave function for all isomers suggests that radical electron coupling takes place via either through-space or 1,3 through-bond coupling, i.e., if through-bond coupling were occurring via the 1,4 motif, this would swap the energetic ordering of these orbitals to favor the $(\sigma^*)^2(\sigma)^0$ configuration.65 ^{5,73} Our detailed analysis below of the natural orbitals for these ground state wave functions also confirms the presence of 1,3 through-bond coupling in these heteroaromatic isomers.

In addition, provided in Table III are values for the vertical singlet-triplet state splitting, ΔE_{ST} , which demonstrate that this property is, at least qualitatively, related to the weights of the $|(\sigma)^2\rangle$ and the $|(\sigma^*)^2\rangle$ determinants within the total ground state wave function. For example, for the five isomers exhibiting ΔE_{ST} of approximately -0.5 eV or smaller in magnitude, $|(\sigma)^2\rangle$ and $|(\sigma^*)^2\rangle$ contribute with weights of ≤68% and >10%, respectively. Alternatively, for the seven isomers with $\Delta E_{\rm ST} \ge 0.87$ eV, the ground state is >77% $|(\sigma)^2\rangle$ and $\leq 9\%$ $|(\sigma^*)^2\rangle$ —and for the four-configurational **23T**, the $|(\sigma^*)^2\rangle$ determinant does not contribute to the total wave function! While $|(\sigma)^2\rangle$ is still the leading determinant in the ground state of 23T, three open-shell determinants contribute with a larger weight to the total ground state wave function of this isomer than $|(\sigma^*)^2\rangle$. Two of these resemble the OSS singly occupying the σ and σ^* orbitals [i.e., akin to Eq. (3)], but the other is one belonging to a different OSS that singly occupies the 15 a' and σ^* orbitals while doubly occupying the σ orbital, namely $|(15a')^{\beta}(\sigma)^{\alpha\beta}(\sigma^*)^{\alpha}\rangle$. As can be seen in Table S-II.B.1, the 15a' orbital in both the α and β manifolds resembles the fully antisymmetric combination of all σ bonding orbitals within the ring itself. Even with this determinant's relatively small contribution to the ground state wave function of 23T at ~2%, its presence at all is notably different from the ground state wave function of o-benzyne, 79 whose analogous "ring σ^* " natural orbital was found to be even more occupied at the CAS(12,12)-PT2(FC)/ccpVTZ level of theory than that species' radical σ natural orbital (cf. the first two orbitals and occupation numbers in the top row of the table included on pp. 7 of the supplementary material for Ref. 79). It is tempting to ascribe the unimportance of the radical σ^* orbital in **23T** to the very short C_2 – C_3 bond length of 1.26 Å, as this orbital exhibits an intraradical nodal plane that bisects the C₂-C₃ bond; however, the same bond in 23F is a trivial 0.01 Å longer, but the ground state for this isomer actually has the largest relative weight of all isomers for the $|(\sigma^*)^2\rangle$ determinant, at 17%. Because the differences in the weight of the $|(\sigma^*)^2\rangle$ determinant in the total ground state wave functions of 23T and 23F are clearly not geometric in origin, we have also obtained the first pair of particle/hole natural transition orbitals (NTOs) for the spin-flip excitations of the highspin reference determinants necessary to generate the ground state wave functions of all isomers to more closely examine the electronic factors that must, therefore, control this phenomenon.

With $N_{\text{occ}} \leq N_{\text{vir}}$ being the number of occupied and virtual (unoccupied) MOs in the reference determinant, respectively, these particle/hole NTOs correspond to the left and right singular vectors of the state-specific transition density matrix T connecting the reference and excited state,80

$$\mathbf{UTV}^{\dagger} = \mathbf{\Lambda},\tag{5}$$

where U and V are unitary transformation matrices within the occupied and virtual MO subspaces of dimension $N_{\rm occ} \times N_{\rm occ}$ and $N_{\rm vir} \times N_{\rm vir}$, and T and Λ are both of dimension $N_{\rm occ} \times N_{\rm vir}$. The positive semidefinite matrix Λ takes the generalized diagonal form

$$\mathbf{\Lambda} = \operatorname{diag}(\lambda_1, \lambda_2, \dots \lambda_N; \mathbf{0}), \tag{6}$$

where each real, positive singular value λ_i is the amplitude for the excitation connecting the particle NTO u_i with the hole NTO v_i . Because the particle NTOs $\{u_i\}$ and the excitation amplitudes $\{\lambda_i\}$ have been shown to be equivalent to the natural orbitals (NOs) $\{|\phi_i\rangle\}$ and the occupation numbers $\{n_i\}$ of the excited state, ⁸¹ we will hereafter refer to them as such for the ground state wave functions listed in Table III. Furthermore, because the transition density matrix T is constructed in the basis of all singly excited determinants with

TABLE IV. Occupation numbers for the σ and σ^* natural orbitals in α and β manifolds $[n_{\phi}(\alpha)$ and $n_{\phi}(\beta)$ for the generic orbital label ϕ , respectively] computed for the ground state wave functions of each diradical isomer at the EOM-SF-UCCSD/cc-pVDZ level of theory with their S₁ structure. In addition, provided for convenience are effective total occupations $n_{\phi} = n_{\phi}(\alpha) + n_{\phi}(\beta)$ for σ and σ^* natural orbitals, as well as the difference of these effective total populations, $\Delta n = n_{\sigma} - n_{\sigma*}$, and the number of effectively unpaired electrons according to the Head–Gordon index, ^{82,83} $n_{u,n}$.

Isomer	Orbital	$n_{\phi}(\alpha)$	$n_{\phi}(\beta)$	$n_{\phi}(\alpha) + n_{\phi}(\beta)$	$n_{\sigma}-n_{\sigma^*}$	$n_{u,nl}$
23F	σ*	0.214	0.186	0.400	1.183	1.29
	σ	0.805	0.778	1.583		
23T	σ^*	0.059	0.039	0.097	1.791	0.09
	σ	0.953	0.935	1.888		
23P	σ^*	0.212	0.185	0.397	1.191	0.86
	σ	0.805	0.783	1.588	1.171	0.00
24F	σ^*	0.159	0.139	0.298	1.385	0.58
	σ	0.853	0.830	1.683	1.363	
24T	σ^*	0.202	0.180	0.383	1 210	0.05
	σ	0.811	0.781	1.592	1.210	0.85
24P	σ^*	0.133	0.115	0.248	1.485	0.42
241	σ	0.877	0.856	1.734	1.403	0.42
25F	σ^*	0.294	0.267	0.560	0.858	1.34
231	σ	0.727	0.691	1.419	0.030	1.54
25T	σ^*	0.163	0.141	0.304	1.372	0.57
	σ	0.852	0.825	1.676	1.3/2	0.57
25P	σ^*	0.261	0.237	0.497	0.985	1.15
	σ	0.757	0.726	1.483	0.763	
34F	σ*	0.148	0.127	0.274	1 427	0.47
	σ	0.866	0.846	1.711	1.437	
34T	σ^*	0.131	0.108	0.239	1 502	0.38
	σ	0.883	0.859	1.742	1.503	
	$\overline{\sigma^*}$	0.136	0.116	0.252	1 402	0.41
34P	σ	0.876	0.859	1.735	1.483	0.41

nonzero contribution to the desired excited state (i.e., whose excitation amplitudes are nonzero), $\{|\phi_i\rangle\}$ and $\{n_i\}$ for each ground state wave function include contributions from all determinants with nonzero weight in the multiconfigurational expansions of Table III. Of particular interest to the following discussion are the radical σ and σ^* NOs, which we have included in Tables S-III.A.1–S-III.C.4 of the supplementary material, and whose occupation numbers we have listed in Table IV. By comparing the σ^* NOs for 23F and 23T, it is clear that the lobe of σ^* surrounding C_2 is spatially cramped in 23T by a lobe surrounding the sulfur that is largely absent from the oxygen in 23F. As a result, the σ^* NO is destabilized in 23T relative to 23F, which is consistent with the smaller effective total occupation $[n_{\sigma^*} = n_{\sigma^*}(\alpha) + n_{\sigma^*}(\beta)]$ of 0.097 vs 0.400 for 23T and 23F, respectively.

In addition, provided in Table IV are the effective number of unpaired electrons in each excited state as computed by the Head–Gordon index, $n_{u,nl}$, which is given by

$$n_{u,nl} = \sum \overline{n}_i^2 (2 - \overline{n}_i)^2, \qquad (7)$$

where \overline{n}_i is the spin-averaged occupation number for natural orbital ϕ_i . Clearly, there is a significant breadth in the values of $n_{u,nl}$, ranging

from as small as $0.09e^-$ for 23T to as large as $1.29e^-$ for 23F. Other than for 23T, the ground state wave functions must, therefore, have nontrivial contributions from various OSS states; this is not unexpected given that the TCS-dominated ground state of p-benzyne has $n_{u,nl} = 0.28$ (cf. Table II of Ref. 63). The seemingly surprising value of $n_{u,nl} = 0.09e^-$ for 23T is actually understandable when combining the data in Tables III and IV. From Table III, we can see that 23T is the only diradical isomer for which the $(\sigma^*)^{\alpha\beta}$ configuration does not make a significant contribution to the ground state wave function. Furthermore, from Table IV, the occupation number for the σ^* NO of only 0.097 is the smallest among all diradical isomers. The tiny value of $n_{u,nl}$ for 23T is, therefore, a result of the dominance of the $(\sigma)^{\alpha\beta}$ NO rather than the *lack* of any open-shell determinants in the ground state wave function.

Beyond using the isomer NOs simply to interpret the weights of determinants contributing to the ground state wave functions (Table III), we may also use the NOs and occupation numbers to illuminate the nature of the coupling between radical electrons. In Sec. III A, we attempted to interpret the geometric deformations displayed by these diradical isomers to the presence of either through-space or through-bond coupling between the (nonbonding) radical orbitals σ and σ^* . In so doing, we implicitly assumed a (semi-)localized picture of the bonding in our diradical isomers, 61 similar in spirit to the valence bond theory (VB) perspective of chemical bonding that is ubiquitous in (especially experimental) organic chemistry. Thanks to the simultaneous facts that (i) the ground state wave functions for all diradical isomers can be reasonably interpreted within the classical two-level picture and (ii) that the generalized valence bond (GVB) and two-configurational SCF (TCSCF) description of diradical singlets have been shown to be equivalent,⁷⁸ our semilocal interpretation in Sec. III A is not, as it may appear, actually at odds with the molecular-orbital theory (MO)-based discussion of Sec. III B. Therefore, by reinterpreting our diradical isomers' ground state wave functions (Table III) and their natural orbitals (Tables S-III.A.1-S-III.C.4 of the supplementary material) through a semilocal lens, we may indulge our VBattuned desire for chemical intuition even within the NO framework necessary for quantitative accuracy.

As noted earlier, both through-space and 1,3 through-bond coupling lead to the simultaneous stabilization of the symmetric combination of semilocal radical lobes (the radical σ MO) and destabilization of the corresponding antisymmetric combination (σ^*), thereby favoring a total wave function with electron configuration $(\sigma)^2(\sigma^*)^0$ thanks to the aufbau principle. Unlike molecular orbitals, which can be only "occupied" or "unoccupied," however, any natural orbital (NO) ϕ can be fractionally occupied, where the NO occupation number n_{ϕ} represents the *effective* number of electrons occupying each orbital, varying between 0 and 2 for restricted NOs (or between 0 and 1 for unrestricted NOs) and which collectively sum to the total number of electrons in the molecule. Provided in Table IV are occupation numbers for the σ and σ^* natural orbitals in both the α and β manifolds, denoted by $n_{\phi}(\alpha)$ and $n_{\phi}(\beta)$ for the arbitrary orbital label ϕ . Because $n_{\phi}(\alpha)$ and $n_{\phi}(\beta)$ vary independently of one another and without consideration for chemical interpretation, we also include in Table IV the effective total occupation for each of the σ and σ^* NOs, computed simply as $n_{\phi} = n_{\phi}(\alpha)$ + $n_{\phi}(\beta)$, together with the difference between these total occupations, $\Delta n = n_{\sigma} - n_{\sigma*}$. By analogy to the MO picture, we would

expect that σ^* will be more occupied than σ for systems dominated by 1,4 through-bond coupling (i.e., $0 \le n_{\sigma} < n_{\sigma^*} \le 2$) and σ will be more occupied than σ^* for systems dominated by either through-space or a 1,3-mediated through-bond coupling (i.e., $0 \le n_{\sigma^*} < n_{\sigma} \le 2$). Based on the orbital populations shown in Table IV, where $n_{\sigma^*} < n_{\sigma}$ for all isomers, 1,3-mediated through-bond coupling and/or through-space coupling appears to be the dominant coupling motif in all isomers. These NO populations confirm our prediction in Sec. III A that 1,3-mediated through-bond coupling dominates over 1,4-mediated through-bond coupling for all isomers with the lone exception of 25F. Due to the presence of some confounding subtleties in that isomer, however, we must first discuss another trend, namely the vague relationship between the vertical singlet triplet state splittings and the weights with which $|(\sigma)^2\rangle$ and $|(\sigma^*)^2\rangle$ contribute to each isomer's total ground state wave function.

Within the (2e, 2o) picture, we should expect that σ will be increasingly stabilized and σ^* increasingly destabilized as the strength of either the through-space or 1,3-mediated through-bond coupling between these orbitals increases (such coupling is hereafter denoted as $\sigma \cdot \cdot \cdot \sigma^*$). In this simplified (2e, 2o) framework, $\Delta E_{\rm ST}$ will be related to the difference of the energies of the $(\sigma)^{\beta}$ and $(\sigma^*)^{\alpha}$ orbitals, since at least for the leading $|(\sigma)^2\rangle$ determinant, the $S_0 \leftarrow T_1$ transition is equivalent to the $(\sigma)^{\beta} \leftarrow (\sigma^*)^{\alpha}$ spin-flip excitation. While this is of course not perfectly representative of the many-electron nature of our real molecules, we may apply this logic to interpret our NO populations. Through this lens, where the NO occupation number n_{ϕ} is the eigenvalue, rather than the MO energy ε , $\sigma \cdot \cdot \cdot \sigma^*$ will instead be related to the differences in their respective orbital occupations $\Delta n = n_{\sigma} - n_{\sigma*}$, with stronger $\sigma \cdot \cdot \cdot \sigma^*$ manifesting as a greater Δn , which we have also included in Table IV for each diradical isomer. Based on the variability present in Δn , the $\sigma \cdots \sigma^*$ coupling strength is not uniform with respect to either heteroatom or isomer. By comparing against the vertical singlet-triplet state splittings presented in Table III, however, Δn clearly does correlate to $\Delta E_{\rm ST}$ and indeed exhibits a correlation coefficient $R^2 = 0.8676$ for a simple linear fit of those variables (see Fig. S-III.D.1 in the supplementary material).

For the 25F isomer, all of the electronic descriptors discussed in this section—including the relative contributions of the $|(\sigma)^2\rangle$ and $|(\sigma^*)^2\rangle$ determinants to the total ground state wave function and the effective total NO occupations—are consistent with what would be expected from a 1,3-mediated through-bond coupling. When examining Δn for this isomer vs all others, however, a pattern emerges: **25F** exhibits the smallest Δn of only 0.858, consistent with its ranking as the isomer with the smallest ΔE_{ST} of only 0.2090 eV. 25F also has one of the smallest weights of the $|(\sigma)^2\rangle$ determinant (65%) and the largest weight of the $|(\sigma^*)^2\rangle$ determinant (17%) within the ground state wave function. Collectively, though these electronic descriptors for 25F do suggest 1,3-mediated through-bond coupling, they do so in the least convincing fashion among all diradical isomers considered. Contrasted against the strong geometric evidence for the dominance of 1,4-mediated through-bond coupling in this system, the only reasonable conclusion is that there exists both strong 1,4-mediated through-bond coupling and strong through-space coupling in this isomer. The competition between these two coupling motifs, whose downstream effects on the electronic and geometric structures of this isomer are diametrically opposite one another, makes their isolated interpretation a significant challenge. Fortunately, however, this semilocal (2e, 2o) analysis filters away this convolution and provides a clear chemical interpretation for the properties of this system.

Finally, we note that while some spin contamination arose when preparing the high-spin triplet reference states for the 2,4-diradical isomers, all spin-flipped singlet states are reasonably spin-pure, with a maximal spin contamination of less than 10% for 23F and 24T but only ~3.8% on average. This is true despite the fact that the unrestricted formulation of EOM-SF-UCCSD applied here is neither restricted to produce a spin eigenfunction by construction (as would be guaranteed by the restricted-open-shell formulation, EOM-SF-ROCCSD) nor spin-projected to eliminate spin contamination.

C. Role of aromaticity in stabilizing diradical isomers

We have applied the nucleus-independent chemical shift approach within the gauge-invariant atomic orbital (GIAO) formalism 75,76 to compute isotropic deshieldings as a semiquantitative metric of aromaticity in our diradical isomers. All magnetic metrics of aromaticity are based on the ring current model, where the delocalized π electrons of an aromatic molecule respond to an applied magnetic field by moving around the ring, thereby generating an electric current whose own magnetic field opposes the applied one. In NICS specifically, the isotropic magnetic (de)shielding is computed by a "probe" atom (without either nuclear

TABLE V. Isotropic deshieldings (ppm) for the S_1 structures of each diradical isomer and the S_0 structure of their respective parent molecules, computed via the nucleus-independent chemical shift (NICS) approach at the (BS–U)B3LYP/6-311++G** level of theory. NICS probes were placed at the ring centroid [NICS(0)] and ± 1 Å above and below the ring centroid along the molecule's principal moment of inertia [NICS(± 1)] (see text). In addition, provided for reference are the NICS(-1, 0, +1) values computed using this same approach for benzene.

		NICS index	
Species	-1	0	+1
Furan	-9.3	-12.2	-9.3
23F	-4.9	-11.7	-4.9
24F	-4.4	-5.1	-4.4
25F	-15.3	-63.4	-15.3
34F	-7.1	-19.2	-7.1
Thiophene	-10.0	-13.7	-10.0
23T	-9.6	-25.1	-9.6
24T	-5.3	-8.7	-5.3
25T	-8.3	-30.5	-8.3
34T	-7.3	-14.3	-7.3
Pyrrole	-11.9	-22.6	-11.9
23P	-5.1	-15.7	-5.1
24P	-7.9	-18.2	-7.9
25P	-3.7	-4.4	-3.7
34P	-8.8	-24.4	-8.8
Benzene	-11.1	-8.7	-11.1

charge or basis functions), located at one or more point(s) in space around a molecule noncoincident with any atomic positions. Most commonly, probes are placed at the geometric center of the ring or ±1 Å above and below the geometric center along a vector normal to the ring plane [a.k.a. NICS(0) and NICS(±1), respectively]. For an aromatic molecule like benzene, probes placed at these locations will be shielded by the π electron aromatic ring current and will, therefore, experience a smaller magnetic field than what is applied, as opposed to the perimeter hydrogens, which feel an enhanced magnetic field (sc. a deshielding) due to the ring current. We have employed the generalized approach developed in Ref. 64 to place the NICS(0) and NICS(± 1) probes for our cyclic diradical isomers, which are not perfectly pentagonal, at the non-mass-weighted centroid of ring atoms and ± 1 Å along the ring atoms' principal moment of inertia above and below the ring centroid. Contained in Table V are these isotropic deshieldings for the S₁ structures of all diradical isomers, computed at the B3LYP/6-311++G** level of theory with a BS-UKS reference using Gaussian 16.77 In addition, included for reference are the isotropic deshieldings for the S₀ structures of the fully saturated parent molecules furan, thiophene, and pyrrole, as well as for benzene, computed with the same approach.

As can be seen from the data in Table V, all NICS probes in our diradical isomers experience the negative deshielding (i.e., shielding) indicative of the presence of at least some aromaticity, although these deshielding values vary significantly. In particular, NICS(0) is larger in magnitude than NICS(±1) for all diradical isomers and their parents, whereas the opposite is true for benzene. Furthermore, even among our heterocycles, NICS(0) deshieldings vary significantly in magnitude, ranging from as little as -4.4 for 25P to as large as -63.4 for 25F. This is not to be interpreted as an indication that 25F is sixfold aromatic; rather, the several very large NICS(0) deshieldings are likely due to the proximity of this probe to the σ bonding network between the ring atoms themselves, which also experience an induced ring current in opposition to the applied magnetic field and further shields this probe. In these diradical isomers, the presence of through-bond coupling is likely increasing the in-plane σ electron density. The presence of the σ ring current is known to be a limitation of the NICS(0) index,69 so further assessment of the traditional π aromaticity in our diradical isomers must instead focus on the deshieldings measured at the NICS(±1) probe locations, which are more likely to measure the π ring current alone.

Compared with the NICS(± 1) deshieldings of benzene, all of the saturated parent molecules are qualitatively aromatic, as are 25F, 23T, 25T, and 34P. Considerable as somewhat aromatic are 34F, 34T, and 24P, while the remaining isomers trend closer to nonaromatic [NICS(± 1) > -5]. Interestingly, excluding 25F as a lone outlier, NICS(± 1) also correlates negatively with Δn , where the simple linear regression of these data (neglecting 25F) exhibits a correlation coefficient of $R^2 = 0.7355$ (see Fig. S-III.D.2 in the supplementary material). Based on this relationship, it appears that aromaticity in these systems increases as the σ radical NO becomes more populated. It is certainly possible that this relationship is purely phenomenological, where the simplicity of the BS-UDFT approach used in our NICS computations is more poorly describing the electronic structure of our isomers and, therefore, underestimating their aromaticity as they increase in diradical character (i.e., as Δn decreases). Instead, we hypothesize that the radical σ NO is slightly better able to contribute to the ring current within the

molecular plane, relative to the σ^* NO. We base this supposition on the difference in the shape of the σ and σ^* NOs: in the σ NO there is no node perpendicular to the perimeter of the ring, while this node is present in all radical σ^* NOs. Therefore, the observed correlation between NICS(± 1) and σ NO occupation is actually not due to an increase in the π aromaticity but rather due to the increased ringσ aromaticity yet affecting the apparent magnetic field strength felt by the NICS(± 1) probes. This interpretation is strongly supported by the high degree of positive correlation between the deshieldings measured at NICS(0) and NICS(± 1) probes, where the linear regression across all isomers (including 25F; see Fig. S-III.D.3) shows a correlation coefficient of $R^2 = 0.9234$. This phenomenon also likely caused 25F to be an outlier in the correlation of NICS(± 1) deshieldings vs Δn (see Fig. S-III.D.2 of the supplementary material), as the incredibly strong in-plane ring current for this isomer—evidenced by its NICS(0) deshielding of -63.4 ppm—is still very much felt at the NICS(± 1) probe locations, even a full Ångstrom away from the ring plane. The outlier behavior of 25F may be attributable to 1,4 through-bond coupling, which does not seem to be present in the other heteroaromatic diradical isomers studied here but is present in para-benzyne, which displays a NICS(0) value of -28.6 (computed at the same level of theory as the values in Table V of Ref. 64).

SUMMARY AND CONCLUSIONS

We have characterized the lowest lying singlet and triplet state geometries of the di-dehydro diradical isomers of furan, pyrrole, and thiophene using broken-symmetry unrestricted density functional theory (wB97X-D/cc-pVDZ). We find that all singlet and triplet structures for these isomeric species display $C_{2\nu}$ [(2,5) or (3,4)] or C_s [(2,3) or (2,4)] symmetry geometries on this potential surface. The structural differences between the structures of these diradical isomers and their fully saturated parent molecules are seemingly driven by through-space and 1,3 through-bond coupling of the radical electrons, with the exception of 25F. To account for any possible multiconfigurational character in the singlet wave functions, we utilized the BS-UDFT geometries to perform an EOM-SF-CCSD/cc-pVDZ analysis of the energetics, wave functions, and natural orbitals. Our EOM-SF-CCSD results indicate that the singlet state lies lower in energy than the triplet state. Electronically, the singlet ground state wave function for all of these isomers is at least two configurational, and the leading contributor is always the $|(\sigma)^2\rangle$ determinant, providing further evidence that through-space or 1,3 through-bond coupling dominates the behavior of these systems. We analyzed the natural orbitals and found that the difference in s and s* NO occupations correlates with the vertical singlet-triplet splittings, as well as revealing that 1,4 through-bond coupling may be occurring for the outlier 25F but is countermanding the effects of through-space and 1,3 through-bond coupling. Finally, we also applied nucleus independent chemical shift (NICS) analysis to qualitatively assess aromaticity and found a relatively high degree of variability with some heteroaromatic isomers displaying aromatic, somewhat aromatic, or non-aromatic properties. We suspect that, in this application, the qualitative nature of NICS analysis (which attempts to measure π ring current) is being further complicated by an increase in σ ring current attributable to the presence of through-bond coupling in these diradical isomers.

SUPPLEMENTARY MATERIAL

See the supplementary material for figures visualizing molecular structures for and tables of geometric parameters for BS-UDFT optimized singlet and triplet geometries for all heteroaromatic diradical species along with the fully saturated parent molecules; tabulated vibrational frequencies confirming all species as minima on the BS-UDFT surface; details for how we prepared the triplet reference state for the EOM-SF-CCSD computations; tables containing visualizations relevant frontier molecular orbitals for the high spin triplet reference; tables containing visualizations of natural orbitals and values utilized in the natural orbital analysis of the EOM-SF-CC wave functions; and plots of Δn vs ΔE_{ST} , Δn vs NICS(± 1), and NICS(0) vs NICS(± 1). Further provided for reference are plain-text XYZ files containing the Cartesian coordinates of the molecular structures of all diradical isomers and fully saturated parent molecules, available in the following publicly accessible GitHub repository: https://github.com/Parish-Lab/heteroaromaticdiradicals

ACKNOWLEDGMENTS

C.P. acknowledges support from the National Science Foundation (Grant No. CHE-1800014), the Donors of the American Chemical Society Petroleum Research Fund, the Thomas F. and Kate Miller Jeffress Memorial Trust, and the Floyd D. and Elisabeth S. Gottwald Endowment for partial support of this work. C.P. also acknowledges support from the Camille and Henry Dreyfus Foundation through the receipt of a Henry Dreyfus Teacher-Scholar Award. Z.C., S. M.-G., and J.E.A.-T. acknowledge summer support from the Puryear-Topham-Pierce-Gupton endowment from the Department of Chemistry at the University of Richmond. Z.C. and C.M.F.A. acknowledge summer support from NSF CHE-1800014, C.M.F.A. acknowledges summer support from the Donors of the American Chemical Society Petroleum Research Fund, S. M.-G. acknowledges summer support from the University of Richmond Integrated and Inclusive Science program, and C.M.F.A. acknowledges summer support from the University of Richmond Arts and Sciences Undergraduate Research Committee. D.A.S. further gratefully acknowledges financial support from the U.S. National Science Foundation (Grant No. OAC-2321044). Computational support was provided by George Flanagin, and computational resources were provided, in part, by the MERCURY supercomputer consortium under NSF Grant Nos. CHE-0116435 and CHE-0521063.

AUTHOR DECLARATIONS

Conflict of Interest

The authors have no conflicts to disclose.

Author Contributions

Zhijian Chen: Data curation (supporting); Formal analysis (supporting); Investigation (supporting); Writing – original draft (supporting); Writing – review & editing (supporting). Sebastian Mendoza-Gomez: Data curation (supporting); Formal analysis

(supporting); Investigation (supporting); Writing - review & editing (supporting). Jean E. Azar-Tanguay: Data curation (supporting); Formal analysis (supporting); Investigation (supporting); Writing - review & editing (supporting). Christine M. F. Ancajas: Formal analysis (supporting); Investigation (supporting); Writing – review & editing (supporting). Dominic A. Sirianni: Conceptualization (equal); Data curation (equal); Formal analysis (equal); Funding acquisition (equal); Investigation (equal); Project administration (equal); Resources (equal); Supervision (equal); Validation (equal); Visualization (equal); Writing - original draft (equal); Writing - review & editing (equal). Carol A. Parish: Conceptualization (equal); Data curation (equal); Formal analysis (equal); Funding acquisition (equal); Investigation (equal); Project administration (equal); Resources (equal); Supervision (equal); Validation (equal); Visualization (equal); Writing - original draft (equal); Writing review & editing (equal).

DATA AVAILABILITY

The data that support the findings of this study are available within the article and its supplementary material. Further structural data (plain-text XYZ files) are openly available in the public GitHub repository at https://github.com/ParishLab/heteroaromatic-diradicals.

REFERENCES

¹E. L. Wynder, "Tobacco as a cause of lung cancer: Some reflections," Am. J. Epidemiol. **146**(9), 687–694 (1997).

²Y. Jiang, C. Mingard, S. M. Huber, V. Takhaveev, M. McKeague, S. Kizaki, M. Schneider, N. Ziegler, V. Hürlimann, J. Hoeng, N. Sierro, N. V. Ivanov, and S. J. Sturla, "Quantification and mapping of alkylation in the human genome reveal single nucleotide resolution precursors of mutational signatures," ACS Cent. Sci. 9(3), 362–372 (2023).

³How Tobacco Smoke Causes Disease: The Biology and Behavioral Basis for Smoking-Attributable Disease, A Report of the Surgeon General, edited by D. Sidransky, L. A. Norman, A. McCarthy, and P. L. Taylor (Centers for Disease Control and Prevention (US); National Center for Chronic Disease Prevention and Health Promotion (US); Office on Smoking and Health (US), Atlanta, GA, 2010).

⁴D. F. Church and W. A. Pryor, "Free-radical chemistry of cigarette smoke and its toxicological implications," Environ. Health Perspect. **64**, 111–126 (1985).

⁵N. Gupta, K. Verma, S. Nalla, A. Kulshreshtha, R. Lall, and S. Prasad, "Free radicals as a double-edged sword: The cancer preventive and therapeutic roles of curcumin," Molecules 25(22), 5390 (2020).

⁶M. M. Roessler and E. Salvadori, "Principles and applications of EPR spectroscopy in the chemical sciences," Chem. Soc. Rev. **47**(8), 2534–2553 (2018).

⁷R. Goel, Z. Bitzer, S. M. Reilly, N. Trushin, J. Foulds, J. Muscat, J. Liao, R. J. Elias, and J. P. Richie, "Variation in free radical yields from U.S. marketed cigarettes," Chem. Res. Toxicol. **30**(4), 1038–1045 (2017).

⁸A. K. A. Jaini, L. B. Hughes, M. M. Kitimet, K. J. Ulep, M. C. Leopold, and C. A. Parish, "Halogen bonding interactions for aromatic and nonaromatic explosive detection," ACS Sens. 4(2), 389–397 (2019).

⁹ A. O. Lykhin, S. Ahmadvand, and S. A. Varganov, "Electronic transitions responsible for ${\rm C_{60}}^+$ diffuse interstellar bands," J. Phys. Chem. Lett. **10**(1), 115–120 (2019).

¹⁰Y. Ozaki, K. B. Beć, Y. Morisawa, S. Yamamoto, I. Tanabe, C. W. Huck, and T. S. Hofer, "Advances, challenges and perspectives of quantum chemical approaches in molecular spectroscopy of the condensed phase," Chem. Soc. Rev. 50(19), 10917–10954 (2021).

¹¹M. Abe, "Diradicals," Chem. Rev. **113**(9), 7011–7088 (2013).

- ¹²X. Lopez, F. Ruipérez, M. Piris, J. M. Matxain, and J. M. Ugalde, "Diradicals and diradicaloids in natural orbital functional theory," ChemPhysChem 12(6), 1061–1065 (2011).
- ¹³C. Shu, Z. Yang, and A. Rajca, "From stable radicals to thermally robust high-spin diradicals and triradicals," Chem. Rev. 123(20), 11954–12003 (2023).
 ¹⁴V. Jung and M. Hard, C. J. "Y. Yang, and M. Hard, C. "Y. Yang, and M. Yang, and A. Yang, and A.
- ¹⁴Y. Jung and M. Head-Gordon, "How diradicaloid is a stable diradical?," ChemPhysChem 4(5), 522–525 (2003).
- ¹⁵ A. Rajca, "Organic diradicals and polyradicals: From spin coupling to magnetism?," Chem. Rev. 94(4), 871–893 (1994).
- ¹⁶N. M. Gallagher, A. Olankitwanit, and A. Rajca, "High-spin organic molecules," J. Org. Chem. 80(3), 1291–1298 (2015).
- 17 Z. Zeng, X. Shi, C. Chi, J. T. López Navarrete, J. Casado, and J. Wu, "Proaromatic and anti-aromatic π -conjugated molecules: An irresistible wish to be diradicals," Chem. Soc. Rev. **44**(18), 6578–6596 (2015).
- ¹⁸B. Alexander Voigt, T. Steenbock, and C. Herrmann, "Structural diradical character," J. Comput. Chem. 40(7), 854–865 (2019).
- ¹⁹L. Salem and C. Rowland, "The electronic properties of diradicals," Angew. Chem., Int. Ed. Engl. 11(2), 92–111 (1972).
- M. Winkler and W. Sander, "Triradicals," Acc. Chem. Res. 47(1), 31–44 (2014).
 T. Stuyver, B. Chen, T. Zeng, P. Geerlings, F. De Proft, and R. Hoffmann, "Do diradicals behave like radicals?," Chem. Rev. 119(21), 11291–11351 (2019).
- ²²L. V. Slipchenko and A. I. Krylov, "Singlet-triplet gaps in diradicals by the spinflip approach: A benchmark study," J. Chem. Phys. **117**(10), 4694–4708 (2002).
- ²³A. Hinz, J. Bresien, F. Breher, and A. Schulz, "Heteroatom-based diradical(oid)s," Chem. Rev. **123**(16), 10468–10526 (2023).
- ²⁴A. Das, T. Müller, F. Plasser, D. B. Krisiloff, E. A. Carter, and H. Lischka, "Local electron correlation treatment in extended multireference calculations: Effect of acceptor–donor substituents on the biradical character of the polycyclic aromatic hydrocarbon heptazethrene," J. Chem. Theory Comput. 13(6), 2612–2622 (2017).
- ²⁵B. O. Roos, "Multiconfigurational quantum chemistry for ground and excited states," in *Radiation Induced Molecular Phenomena in Nucleic Acids: A Comprehensive Theoretical and Experimental Analysis*, edited by M. K. Shukla and J. Leszczynski (Springer Netherlands, Dordrecht, 2008), pp. 125–156.
- ²⁶ D. Roca-Sanjuán, F. Aquilante, and R. Lindh, "Multiconfiguration second-order perturbation theory approach to strong electron correlation in chemistry and photochemistry," WIRES Comput. Mol. Sci. 2(4), 585–603 (2012).
- ²⁷R. Izsák, A. V. Ivanov, N. S. Blunt, N. Holzmann, and F. Neese, "Measuring electron correlation: The impact of symmetry and orbital transformations," J. Chem. Theory Comput. **19**(10), 2703–2720 (2023).
- ²⁸G. K.-L. Chan, J. J. Dorando, D. Ghosh, J. Hachmann, E. Neuscamman, H. Wang, and T. Yanai, "An introduction to the density matrix renormalization group ansatz in quantum chemistry," in *Frontiers in Quantum Systems in Chemistry and Physics* (Springer, Netherlands, Dordrecht, 2008), pp. 49–65.
- ²⁹ P. G. Szalay, T. Müller, G. Gidofalvi, H. Lischka, and R. Shepard, "Multiconfiguration self-consistent field and multireference configuration interaction methods and applications," Chem. Rev. 112(1), 108–181 (2012).
- ³⁰ A. E. Torres, P. Guadarrama, and S. Fomine, "Multiconfigurational character of the ground states of polycyclic aromatic hydrocarbons. A systematic study," J. Mol. Model. 20(5), 2208 (2014).
- ³¹ D. I. Lyakh, M. Musiał, V. F. Lotrich, and R. J. Bartlett, "Multireference nature of chemistry: The coupled-cluster view," Chem. Rev. 112(1), 182–243 (2012).
- ³²Y. Damour, A. Scemama, D. Jacquemin, F. Kossoski, and P.-F. Loos, "State-specific coupled-cluster methods for excited states," J. Chem. Theory Comput. 20(10), 4129–4145 (2024).
- ³³M. Saitow, Y. Kurashige, and T. Yanai, "Fully internally contracted multireference configuration interaction theory using density matrix renormalization group: A reduced-scaling implementation derived by computer-aided tensor factorization," J. Chem. Theory Comput. 11(11), 5120–5131 (2015).
- ³⁴S. Nishihara, T. Saito, S. Yamanaka, Y. Kitagawa, T. Kawakami, M. Okumura, and K. Yamaguchi, "MkMRCC, APUCC and APUBD approaches to 1,n-didehydropolyene diradicals: The nature of through-bond exchange interactions," Mol. Phys. **108**(19–20), 2559–2578 (2010).
- 35 K. Yamaguchi, S. Yamanaka, J. Shimada, H. Isobe, T. Saito, M. Shoji, Y. Kitagawa, and M. Okumura, "Extended Hartree–Fock theory of chemical reactions. IX. Diradical and perepoxide mechanisms for oxygenations of ethylene with

- molecular oxygen and iron-oxo species are revisited," Int. J. Quantum Chem. 109(15), 3745-3766 (2009).
- ³⁶S. Chattopadhyay, "*Ab initio* probing of the ground state of tetraradicals: Breakdown of Hund's multiplicity rule," J. Phys. Chem. A **123**(11), 2211–2226 (2019).
- ³⁷S. Chattopadhyay, U. S. Mahapatra, and R. K. Chaudhuri, "Investigation of low-lying states of oxygen molecule via second-order multireference perturbation theory: A state-specific approach," J. Phys. Chem. A 113(20), 5972–5984 (2009).
- ³⁸S. Sinha Ray, A. Ghosh, S. Chattopadhyay, and R. K. Chaudhuri, "Taming the electronic structure of diradicals through the window of computationally cost effective multireference perturbation theory," J. Phys. Chem. A **120**(29), 5897–5916 (2016).
- ³⁹F. Neese, "Definition of corresponding orbitals and the diradical character in broken symmetry DFT calculations on spin coupled systems," J. Phys. Chem. Solids **65**(4), 781–785 (2004).
- ⁴⁰J.-M. Mouesca, "Density functional theory-broken symmetry (DFT-BS) methodology applied to electronic and magnetic properties of bioinorganic prosthetic groups," Methods Mol. Biol. 1122, 269–296 (2014).
- ⁴¹N. Ferré, N. Guihéry, and J.-P. Malrieu, "Spin decontamination of brokensymmetry density functional theory calculations: Deeper insight and new formulations," Phys. Chem. Chem. Phys. **17**(22), 14375–14382 (2015).
- ⁴²T. D. Crawford, E. Kraka, J. F. Stanton, and D. Cremer, "Problematic *p*-benzyne: Orbital instabilities, biradical character, and broken symmetry," J. Chem. Phys. 114(24), 10638–10650 (2001).
- ⁴³J. Gräfenstein, E. Kraka, M. Filatov, and D. Cremer, "Can unrestricted density-functional theory describe open shell singlet biradicals?," Int. J. Mol. Sci. 3(4), 360–394 (2002).
- ⁴⁴L. Noodleman, "Valence bond description of antiferromagnetic coupling in transition metal dimers," J. Chem. Phys. **74**(10), 5737–5743 (1981).
- ⁴⁵Y. Horbatenko, S. Sadiq, S. Lee, M. Filatov, and C. H. Choi, "Mixed-reference spin-flip time-dependent density functional theory (MRSF-TDDFT) as a simple yet accurate method for diradicals and diradicaloids," J. Chem. Theory Comput. 17(2), 848–859 (2021).
- ⁴⁶ H. Li, Z. Pu, Q. Sun, Y. Q. Gao, and Y. Xiao, "Noncollinear and spin-flip TDDFT in multicollinear approach," J. Chem. Theory Comput. 19(8), 2270–2281 (2023).
- ⁴⁷Y. Shao, M. Head-Gordon, and A. I. Krylov, "The spin-flip approach within time-dependent density functional theory: Theory and applications to diradicals," J. Chem. Phys. **118**(11), 4807–4818 (2003).
- ⁴⁸Y. A. Bernard, Y. Shao, and A. I. Krylov, "General formulation of spin-flip time-dependent density functional theory using non-collinear kernels: Theory, implementation, and benchmarks," J. Chem. Phys. **136**(20), 204103 (2012).
- ⁴⁹S. Lee, M. Filatov, S. Lee, and C. H. Choi, "Eliminating spin-contamination of spin-flip time dependent density functional theory within linear response formalism by the use of zeroth-order mixed-reference (MR) reduced density matrix," J. Chem. Phys. **149**(10), 104101 (2018).
- ⁵⁰ A. I. Krylov, "Spin-flip configuration interaction: An electronic structure model that is both variational and size-consistent," Chem. Phys. Lett. **350**(5–6), 522–530 (2001).
- ⁵¹D. Casanova and M. Head-Gordon, "The spin-flip extended single excitation configuration interaction method," J. Chem. Phys. 129(6), 064104 (2008).
- ⁵²X. Zhang and J. M. Herbert, "Spin-flip, tensor equation-of-motion configuration interaction with a density-functional correction: A spin-complete method for exploring excited-state potential energy surfaces," J. Chem. Phys. **143**(23), 234107 (2015).
- 53 A. I. Krylov, "Size-consistent wave functions for bond-breaking: The equation-of-motion spin-flip model," Chem. Phys. Lett. 338(4-6), 375–384 (2001).
- ⁵⁴A. I. Krylov and C. D. Sherrill, "Perturbative corrections to the equation-of-motion spin-flip self-consistent field model: Application to bond-breaking and equilibrium properties of diradicals," J. Chem. Phys. 116(8), 3194–3203 (2002).
 ⁵⁵L. V. Slipchenko and A. I. Krylov, "Spin-conserving and spin-flipping equation-
- ⁵⁵L. V. Slipchenko and A. I. Krylov, "Spin-conserving and spin-flipping equation-of-motion coupled-cluster method with triple excitations," J. Chem. Phys. **123**(8), 084107 (2005).
- ⁵⁶J. S. Sears, C. D. Sherrill, and A. I. Krylov, "A spin-complete version of the spin-flip approach to bond breaking: What is the impact of obtaining spin eigenfunctions?," J. Chem. Phys. 118(20), 9084–9094 (2003).

- ⁵⁷A. I. Krylov, "Spin-flip equation-of-motion coupled-cluster electronic structure method for a description of excited states, bond breaking, diradicals, and triradicals," ChemInform 37(17), 83–91 (2006).
- ⁵⁸ A. I. Krylov, "Equation-of-motion coupled-cluster methods for open-shell and electronically excited species: The Hitchhiker's guide to Fock space," Annu. Rev. Phys. Chem. **59**(1), 433–462 (2008).
- ⁵⁹ P. U. Manohar and A. I. Krylov, "A noniterative perturbative triples correction for the spin-flipping and spin-conserving equation-of-motion coupled-cluster methods with single and double substitutions," J. Chem. Phys. **129**(19), 194105 (2008).
- ⁶⁰S. V. Levchenko and A. I. Krylov, "Equation-of-motion spin-flip coupled-cluster model with single and double substitutions: Theory and application to cyclobutadiene," J. Chem. Phys. 120(1), 175–185 (2004).
- ⁶¹ N. Orms and A. I. Krylov, "Singlet-triplet energy gaps and the degree of diradical character in binuclear copper molecular magnets characterized by spin-flip density functional theory," Phys. Chem. Chem. Phys. 20(19), 13127–13144 (2018).
 ⁶² I. Badía-Domínguez, S. Canola, V. Hernández Jolín, J. T. López Navarrete, J. C. Sancho-García, F. Negri, and M. C. Ruiz Delgado, "Tuning the diradical character of indolocarbazoles: Impact of structural isomerism and substitution position," J. Phys. Chem. Lett. 13(26), 6003–6010 (2022).
- ⁶³ A. R. Luxon, N. Orms, R. Kanters, A. I. Krylov, and C. A. Parish, "An *ab initio* exploration of the Bergman cyclization," J. Phys. Chem. A 122(1), 420–430 (2018).
 ⁶⁴ D. A. Sirianni, X. Song, S. Wairegi, E. B. Wang, S. A. Mendoza-Gomez, A. Luxon, M. Zimmerley, A. Nussdorf, M. Filatov, R. Hoffmann, and C. A. Parish, "Variations on the Bergman cyclization theme: Electrocyclizations of ionic penta-hepta-and octadiynes," J. Am. Chem. Soc. 145(39), 21408–21418 (2023).
 ⁶⁵ D. L. G. L. G.
- ⁶⁵R. Hoffmann, "Interaction of orbitals through space and through bonds," Acc. Chem. Res. 4(1), 1–9 (1971).
- ⁶⁶ P. v. R. Schleyer, C. Maerker, A. Dransfeld, H. Jiao, and N. J. R. van Eikema Hommes, "Nucleus-independent chemical shifts: A simple and efficient aromaticity probe," J. Am. Chem. Soc. 118(26), 6317–6318 (1996).
- ⁶⁷Z. Chen, C. S. Wannere, C. Corminboeuf, R. Puchta, and P. v. R. Schleyer, "Nucleus-independent chemical shifts (NICS) as an aromaticity criterion," Chem. Rev. 105(10), 3842–3888 (2005).
- ⁶⁸ E. Paenurk and R. Gershoni-Poranne, "Simple and efficient visualization of aromaticity: Bond currents calculated from NICS values," Phys. Chem. Chem. Phys. 24, 8631 (2022).
- ⁶⁹R. Gershoni-Poranne and A. Stanger, "NICS—Nucleus independent chemical shift," in *Aromaticity: Modern Computational Methods and Applications*, 1st ed., edited by I. Fernandez (Elsevier, Cambridge, 2021).
- ⁷⁰J.-D. Chai and M. Head-Gordon, "Long-range corrected hybrid density functionals with damped atom-atom dispersion corrections," Phys. Chem. Chem. Phys. 10(44), 6615–6620 (2008).
- ⁷¹J.-D. Chai and M. Head-Gordon, "Systematic optimization of long-range corrected hybrid density functionals," J. Chem. Phys. 128(8), 084106 (2008).
- ⁷²T. H. Dunning, Jr., "Gaussian basis sets for use in correlated molecular calculations. I. The atoms boron through neon and hydrogen," J. Chem. Phys. **90**(2), 1007–1023 (1989).
- ⁷³R. Hoffmann, A. Imamura, and W. J. Hehre, "Benzynes, dehydroconjugated molecules, and the interaction of orbitals separated by a number of intervening sigma bonds," J. Am. Chem. Soc. 90(6), 1499–1509 (1968).
- ⁷⁴Y. Shao, Z. Gan, E. Epifanovsky, A. T. B. Gilbert, M. Wormit, J. Kussmann, A. W. Lange, A. Behn, J. Deng, X. Feng, D. Ghosh, M. Goldey, P. R. Horn, L. D. Jacobson, I. Kaliman, R. Z. Khaliullin, T. Kuś, A. Landau, J. Liu, E. I. Proynov, Y. M. Rhee, R. M. Richard, M. A. Rohrdanz, R. P. Steele, E. J. Sundstrom, H. L. Woodcock, P. M. Zimmerman, D. Zuev, B. Albrecht, E. Alguire, B. Austin, G. J. O. Beran, Y. A. Bernard, E. Berquist, K. Brandhorst, K. B. Bravaya, S. T. Brown, D. Casanova, C.-M. Chang, Y. Chen, S. H. Chien, K. D. Closser, D. L. Crittenden, M. Diedenhofen, R. A. DiStasio, H. Do, A. D. Dutoi, R. G. Edgar, S. Fatehi, L. Fusti-Molnar, A. Ghysels, A. Golubeva-Zadorozhnaya, J. Gomes, M. W. D. Hanson-Heine, P. H. P. Harbach, A. W. Hauser, E. G. Hohenstein, Z. C. Holden,

- T.-C. Jagau, H. Ji, B. Kaduk, K. Khistyaev, J. Kim, J. Kim, R. A. King, P. Klunzinger, D. Kosenkov, T. Kowalczyk, C. M. Krauter, K. U. Lao, A. D. Laurent, K. V. Lawler, S. V. Levchenko, C. Y. Lin, F. Liu, E. Livshits, R. C. Lochan, A. Luenser, P. Manohar, S. F. Manzer, S.-P. Mao, N. Mardirossian, A. V. Marenich, S. A. Maurer, N. J. Mayhall, E. Neuscamman, C. M. Oana, R. Olivares-Amaya, D. P. O'Neill, J. A. Parkhill, T. M. Perrine, R. Peverati, A. Prociuk, D. R. Rehn, E. Rosta, N. J. Russ, S. M. Sharada, S. Sharma, D. W. Small, A. Sodt, T. Stein, D. Stück, Y.-C. Su, A. J. W. Thom, T. Tsuchimochi, V. Vanovschi, L. Vogt, O. Vydrov, T. Wang, M. A. Watson, J. Wenzel, A. White, C. F. Williams, J. Yang, S. Yeganeh, S. R. Yost, Z.-Q. You, I. Y. Zhang, X. Zhang, Y. Zhao, B. R. Brooks, G. K. L. Chan, D. M. Chipman, C. J. Cramer, W. A. Goddard, M. S. Gordon, W. J. Hehre, A. Klamt, H. F. Schaefer, M. W. Schmidt, C. D. Sherrill, D. G. Truhlar, A. Warshel, X. Xu, A. Aspuru-Guzik, R. Baer, A. T. Bell, N. A. Besley, J.-D. Chai, A. Dreuw, B. D. Dunietz, T. R. Furlani, S. R. Gwaltney, C.-P. Hsu, Y. Jung, J. Kong, D. S. Lambrecht, W. Liang, C. Ochsenfeld, V. A. Rassolov, L. V. Slipchenko, J. E. Subotnik, T. Van Voorhis, J. M. Herbert, A. I. Krylov, P. M. W. Gill, and M. Head-Gordon, "Advances in molecular quantum chemistry contained in the Q-Chem 4 program package," Mol. Phys. 113(2), 184–215 (2015).

 75 R. M. Aminova, H. I. Zoroatskaya, and Y. Y. Samitov, "Calculation of
- ⁷⁵R. M. Aminova, H. I. Zoroatskaya, and Y. Y. Samitov, "Calculation of nuclear magnetic shielding constants by the method of gauge-invariant atomic orbitals using Gaussian functions," J. Magn. Reson. (1969) 33(3), 497–503 (1979).
- ⁷⁶K. Wolinski, J. F. Hinton, and P. Pulay, "Efficient implementation of the gauge-independent atomic orbital method for NMR chemical shift calculations," J. Am. Chem. Soc. 112(23), 8251–8260 (1990).
- ⁷⁷ M. J. Frisch, G. W. Trucks, H. B. Schlegel, G. E. Scuseria, M. A. Robb, J. R. Cheeseman, G. Scalmani, V. Barone, G. A. Petersson, H. Nakatsuji, X. Li, M. Caricato, A. V. Marenich, J. Bloino, B. G. Janesko, R. Gomperts, B. Mennucci, H. P. Hratchian, J. V. Ortiz, A. F. Izmaylov, J. L. Sonnenberg, F. Ding, F. Lipparini, F. Egidi, J. Goings, B. Peng, A. Petrone, T. Henderson, D. Ranasinghe, V. G. Zakrzewski, J. Gao, N. Rega, G. Zheng, W. Liang, M. Hada, M. Ehara, K. Toyota, R. Fukuda, J. Hasegawa, M. Ishida, T. Nakajima, Y. Honda, O. Kitao, H. Nakai, T. Vreven, K. Throssell, J. A. Jr. Montgomery, J. E. Peralta, F. Ogliaro, M. J. Bearpark, J. J. Heyd, E. N. Brothers, K. N. Kudin, V. N. Staroverov, T. A. Keith, R. Kobayashi, J. Normand, K. Raghavachari, A. P. Rendell, J. C. Burant, S. S. Ijengar, J. Tomasi, M. Cossi, J. M. Millam, M. Klene, C. Adamo, R. Cammi, J. W. Ochterski, R. L. Martin, K. Morokuma, O. Farkas, J. B. Foresman, D. J. Fox et al., Gaussian 16, Revision C.01, Gaussian, Inc., Wallingford, CT, 2016.
- ⁷⁸H. Wei, D. A. Hrovat, Y. Mo, R. Hoffmann, and W. T. Borden, "The contributions of through-bond interactions to the singlet–triplet energy difference in 1,3-dehydrobenzene," J. Phys. Chem. A 113(38), 10351–10358 (2009).
- ⁷⁹G. Ghigo, A. Maranzana, and G. Tonachini, "o-benzyne fragmentation and isomerization pathways: A CASPT2 study," Phys. Chem. Chem. Phys. **16**(43), 23944–23951 (2014).
- ⁸⁰I. Mayer, "Using singular value decomposition for a compact presentation and improved interpretation of the CIS wave functions," Chem. Phys. Lett. **437**(4–6), 284–286 (2007).
- ⁸¹ P. R. Surján, "Natural orbitals in CIS and singular-value decomposition," Chem. Phys. Lett. 439(4–6), 393–394 (2007).
- ⁸² M. Head-Gordon, "Characterizing unpaired electrons from the one-particle density matrix," Chem. Phys. Lett. 372(3-4), 508-511 (2003).
- ⁸³ K. Takatsuka, T. Fueno, and K. Yamaguchi, "Distribution of odd electrons in ground-state molecules," Theoret. Chim. Acta 48(3), 175–183 (1978).
- ground-state molecules," Theoret. Chim. Acta 48(3), 175–183 (1978).

 84 R. McWeeny, "Ring currents and proton magnetic resonance in aromatic molecules," Mol. Phys. 1(4), 311–321 (1958).
- ⁸⁵J. A. Pople, "Molecular orbital theory of aromatic ring currents," Mol. Phys. 1(2), 175–180 (1958).
- ⁸⁶F. London, "Théorie quantique des courants interatomiques dans les combinaisons aromatiques," J. Phys. Radium 8(10), 397–409 (1937).
- ⁸⁷T. Dickens and R. Mallion, "Topological ring-currents in conjugated systems," MATCH Commun. Math. Comput. Chem 76, 297–356 (2016).